FLUID DYNAMICS ASSESSMENT OF THE TESLA TURBINE ROTOR

by

Giampaolo MANFRIDA [*] ***and Lorenzo TALLURI***

Department of Industrial Engineering, University of Florence, Florence, Italy

Original scientific paper
https://doi.org/10.2298/TSCI160601170M

The Tesla turbine seems to offer several points of attractiveness when applied to low-power applications. Indeed, it is a simple, reliable, and low cost machine. The principle of operation of the turbine relies on the exchange of momentum due to the shear forces originated by the flow of the fluid through a tight gap among closely stacked disks.

This turbine was firstly developed by Tesla at the beginning of the 20th century, but it did not stir up much attention due to the strong drive towards large centralized power plants, on the other hand, in recent years, as micro power generation gained attention on the energy market place, this original expander raised renewed interest. The mathematical model of the Tesla turbine rotor is revised, and adapted to real gas operation. The model is first validated by comparison with other assessed literature models. The optimal configuration of the rotor geometry is then investigated running a parametric analysis of the fundamental design parameters. High values of efficiency (isolated rotor) were obtained for the optimal configuration of the turbine, which appears interesting for small-scale power generation. The rotor efficiency depends on the configuration of the disks, particularly on the gap and on the outlet diameter, which determines largely the kinetic energy at discharge.

Key words: *Tesla turbine, mathematical model, rotor efficiency*

Micro generation and the Tesla turbine

In recent years, distributed micro generation of power has become of paramount consideration by industries, governments, and research institutions.

One of the main problems of micro generation of power in thermal energy conversion applications is related to the expander, as this component often presents high manufacturing costs and low reliability. The Tesla turbine seems to tackle these problems. Its simple structure ensures a very reliable and low-cost machine.

The bladeless turbine was first patented by Tesla in 1913 [1]. The first description of the Tesla turbine was given in the patent, fig. 1. It can be described as a multiple parallel flat rigid disks assembly connected to a rotating shaft. The disks are arranged co-axially in order to maintain a very small gap between them. The radial-inflow admission of the working fluid is from one or more tangential nozzles, providing a strong tangential component. The working fluid moves from the inlet to the outlet radius due to the difference in pressure determined by friction and by the exchange of momentum, and exits from openings made on the disks and/or shaft at the inner radius.

* Corresponding author, e-mail: giampaolo.manfrida@unifi.it

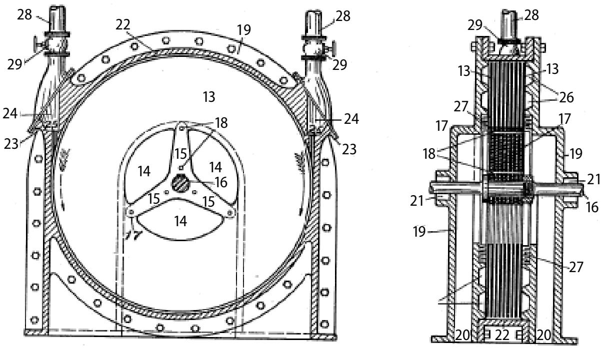

Figure 1. Figures from the patent of Tesla, 1913 [1]

The Tesla turbine did not encounter much success when it was proposed, and eventually it was not investigated deeply and further developed for a long time.

Only in the 1950s Armstrong built an experimental test rig to investigate the performance of the disk turbine [2]. He conducted a test campaign, with steam as working fluid and different nozzle configurations. A valuable result was the understanding of one of the causes of inefficiency. Indeed, it was found that the nozzle flow strongly affects the performance of the turbine.

After the Armstrong tests the Tesla turbine was not investigated for another 15 years. Only with Rice [3], a sound analytic/numerical model, based on the physics of the flow, was developed. The radial velocity rises proceeding towards the centre due to the reduction of the flow area. The tangential velocity is determined by the local balance of the force components (momentum/friction). The mathematical model performed a notable simplification of the Navier-Stokes equations, allowing tackling the solution with the first computers available at the time. The main assumptions were to consider steady flow of an inviscid incompressible working fluid. Rice also built and tested six different types of disk turbines, with air as working fluid.

After Rice's pioneer work, research on the Tesla turbine was set aside until recent times. Lately, new research has flourished on the subject.

Hoya and Guha [4] designed and built a new test rig for measuring the output torque and power of a Tesla turbine. In their work Guha and Smiley [5], investigated the nozzle recognizing it as the source of the major irreversibility according to their test results. They demonstrated that a careful design of the nozzle could reduce the nozzle losses by 40-50%. Also Neckel and Godinho [6] focused their research on nozzle geometry. In their research ten nozzles were designed, manufactured and tested with air as working fluid. Their study confirmed that the nozzle is the critical component of the turbine and that an adequate design could contribute to increase the overall efficiency of the turbine.

Carey [7] presented an assessment of the disc turbine for a small-scale application. He developed an analytical solution of the governing equations, declaring an achievable isentropic efficiency of 75% in optimal design conditions. A complete computational and theoretical modelling of the flow inside a Tesla turbine was presented by Carey [8]. In this work, he fully explains the advantages and drawbacks of computational and analytical analysis. Furthermore, Carey also discusses the advantages of using this expander for green-energy applications. Guha and Sengupta [9] and Sengupta and Guha [10] developed an accurate fluid dynamics model of the turbine, considering individually the role of each force (centrifugal, Coriolis, inertial, and viscous). Lemma *et al.* [11] and Guha and Sengupta [12], also developed a CFD analysis and a general characterization of the performance of the Tesla turbine.

The development of a micro Tesla turbine was investigated by Romanin *et al.* [13]. In this study, the experimental data showed that a 1 cm rotor could achieve an efficiency of 36%. Starting from these data, Krishan *et al.* [14] developed scaling laws and gave recommendations for the development of a 1 mm Tesla turbine. Guha and Sengupta [15] also developed a similitude study on the flow of the Tesla turbine. The scaling laws were obtained through the Buckingham Pi theorem, which lead to the definition of seven fundamental non-dimensional numbers. A further study of Guha and Sengupta [16] demonstrated that the application of the Euler turbomachinery equation is consistent only if local velocity mass-averaged values are considered. Recent published work on the Tesla turbine deals with the investigation of nanofluids applications [17], an increase of power output of 30% appears to be possible when the volume fraction of nanoparticles is increased from 0 to 0.05.

There are several interesting studies on experimental tests of Tesla turbines and on the development of its flow model. However, there still exists a literature gap on the fluid dynamics analysis of the rotor for compressible fluids, as well as for real-fluid effects which are likely using refrigerants or advanced working fluids utilized for low-power and low-temperature applications.

Therefore, the principal aim of this study is to build a mathematical model of the rotor in order to assess the correct geometry, as well as to assemble a numerical tool to evaluate the performance of the Tesla turbine.

Model of the rotor flow

General flow equations and assumptions

The model for the rotor flow is derived from [3, 7, 9] with some relevant changes.
- The hypothesis of incompressible flow with constant density is removed.
- Density – as well as all other thermodynamic functions – is taken as a fluid property depending on the local variables (typically, pressure, and temperature).
- A real fluid model is applied (no perfect gas assumptions).

Because of these assumptions, the equations are solved numerically with fluid properties locally evaluated by engineering equation solver (EES). Furthermore, in order to develop a sound analytical model, additional assumptions have been made.
- Steady, laminar flow.
- The viscous force is treated as a body force acting on the flow at each ($r - \theta$) position.
- The 2-D flow:
  - $V_z = 0$,
  - V_r = constant across the channel, and
  - V_θ = constant across the channel.
- Radial symmetric flow field, uniform at the inlet ($r = r_0$). The flow field is thus the same for any θ, therefore, the derivative $\partial/\partial\theta = 0$ for all flow variables.
- The ($\partial p/\partial\theta$) negligible compared to wall friction forces.

Taking into account the previous assumptions, the fundamental Navier-Stokes equations in cylindrical co-ordinates are reduced to:
- continuity

$$\frac{1}{r}\frac{\partial(r\rho V_r)}{\partial r} = 0 \tag{1}$$

- momentum, r-direction

$$V_r\frac{\partial V_r}{\partial r} - \frac{V_\theta^{\,2}}{r} = -\frac{1}{\rho}\left(\frac{\partial p}{\partial r}\right) + f_r \tag{2}$$

– momentum, θ-direction

$$V_r \frac{\partial V_\theta}{\partial r} + \frac{V_r V_\theta}{r} = f_\theta \tag{3}$$

– momentum, z-direction

$$-\frac{1}{\rho}\left(\frac{\partial p}{\partial z}\right) = 0 \tag{4}$$

The integration of the reduced continuity eq. (1) results in $r\rho V_r = \text{costant}$. Furthermore, knowing the mass-flow rate inside each channel, it follows that locally:

$$V_r = -\frac{\dot{m}_c}{2\pi r b \rho} \tag{5}$$

Formulation of the viscous shear stress

Considering a fluid element between the two disks defining the flow channel, a control volume, V_e, can be defined with base surface, A_e, and height, b. The fluid wetted area is $A_w = 2A_e$. Therefore, the hydraulic diameter, D_h, is equal to $2b$. Consequently:

$$A_e = \frac{Q_e}{b} = \frac{2Q_e}{D_h} \qquad A_w = \frac{4Q_e}{D_h} \tag{6}$$

For laminar flow, the wall shear effect can be expressed as a function of a friction factor ζ and of the relative velocity of the flow. Equation (7) displays the expression of the wall shear stress, decomposing the relative velocity in its two components:

$$\tau_w = \frac{\zeta\rho}{2} w^2 = \frac{\zeta\rho}{2}\left[\left(V_\theta - \omega r\right)^2 + V_r^2\right] \tag{7}$$

Considering $U = (U_0/r_0)r$ and $\zeta = 24/\text{Re}$ as usual for laminar flow between parallel plates:

$$\zeta = \frac{24\mu}{\rho W D_h} = \frac{24\mu}{\rho W D_h} = \frac{24\mu}{\rho D_h \sqrt{\left(V_\theta - \omega r\right)^2 + V_r^2}} \tag{8}$$

So that:

$$\tau_w = \frac{12\mu}{D_h}\sqrt{\left(V_\theta - \omega r\right)^2 + V_r^2} \tag{9}$$

The force resulting from wall friction force is given by the product of the wall shear with the wetted area:

$$F = \frac{12\mu Q_e}{b^2}\sqrt{\left(V_\theta - \omega r\right)^2 + V_r^2} \tag{10}$$

The wall friction force has a tangential and a radial component, which influence respectively the torque and the radial pressure gradient.

Solution of the rotor flow

Figure 2 shows the local velocity triangle of the fluid element inside the rotor.

The radial component of the friction force is given by:

$$F_r = F\cos(\beta) \tag{11}$$

where β is the angle between relative velocity and the radial direction. The value of $\cos(\beta)$ can thus be calculated:

$$\cos(\beta) = \frac{w_r}{w} = \frac{V_r}{\sqrt{\left(V_\theta - \omega r\right)^2 + V_r^2}} \tag{12}$$

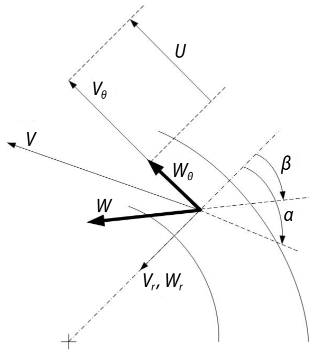

Figure 2. Local velocity triangle

Substituting eq. (12) in eq. (11), a compact expression of the radial force component is obtained:

$$F_r = \frac{12\mu Q_\mathrm{e}}{b^2} V_r \tag{13}$$

Dividing eq. (13) by the mass of the fluid element between two disks, the body force term in the radial direction can be expressed:

$$f_r = \frac{12\mu}{\rho b^2} V_r \tag{14}$$

Proceeding in the same way for the tangential direction, the wall friction force is given by:

$$F_\theta = -F\sin(\beta) \tag{15}$$

$$\sin(\beta) = \frac{w_\theta}{w} = \frac{V_\theta - \omega r}{\sqrt{(V_\theta - \omega r)^2 + V_r^2}} \tag{16}$$

Similarly, substituting eq. (16) in eq. (15), a compact expression of the tangential force is obtained:

$$F_\theta = -\frac{12\mu Q_\mathrm{e}}{b^2}\left(V_\theta - \omega r\right) \tag{17}$$

The body force in tangential direction is thus given by:

$$f_\theta = -\frac{3\mu}{\rho b^2}(V_\theta - \omega r) \tag{18}$$

In order to determine the local pressure, eq. (14) is substituted in eq. (2):

$$V_r \frac{\partial V_r}{\partial r} - \frac{V_\theta^2}{r} = -\frac{1}{\rho}\left(\frac{\partial p}{\partial r}\right) + \frac{12\mu}{\rho b^2} V_r \tag{19}$$

Using eq. (5), the local derivative $(\partial V_r)/\partial r$ can be expressed:

$$\frac{\partial V_r}{\partial r} = -\frac{1}{r} V_r \tag{20}$$

Finally, substituting eq. (20) in eq. (19) the pressure gradient in radial direction is given by:

$$\frac{\partial p}{\partial r}=-\frac{12\mu}{b^2}\left(\frac{\dot{m}_c}{2\pi rb\rho}\right)+\frac{\rho}{r}\left(\frac{\dot{m}_c}{2\pi rb\rho}\right)^2+\frac{\rho}{r}V_\theta^2 \tag{21}$$

Likewise, in order to compute the tangential velocity, eq. (18) can be substituted in eq. (3):

$$V_r\frac{\partial V_\theta}{\partial r}+\frac{V_rV_\theta}{r}=-\frac{12\mu}{\rho b^2}(V_\theta-\omega r) \tag{22}$$

Obtaining finally:

$$\frac{\partial V_\theta}{\partial r}=\frac{24\mu\pi r\left(V_\theta-\omega r\right)}{b\dot{m}_c}-\frac{V_\theta}{r} \tag{23}$$

Which determines the profile of $V_\theta(r)$.

Flow model results – validation

Equations (21) and (23) were programmed into a 2-D (r and θ co-ordinates) EES [18] code with a second-order finite difference approximation. In order to validate the model, it was decided to run the simulations for the same data documented in [3] and for incompressible fluid, tab. 1.

Table 1. Documented data for air as working fluid from [3] and [7]

Inlet rotor total temperature	368 K
Inlet rotor total pressure	101 kPa
Mass-flow rate	0.00194 kg/s
Inlet rotor diameter	0.1778 m
Revolution per minute	6300 rpm

The trends of pressure, tangential and radial velocity of the fluid for variable radius are reported in fig. 3. The radial velocity increases decreasing the radial co-ordinate, according to eq. (5). The tangential velocity profile is determined by two main effects: the conservation of angular momentum (which tends to increase the velocity of the fluid), and viscous forces (which conversely tend to decrease fluid velocity). At high x_i values, viscous forces are predominant, whereas the conservation of angular momentum prevails at low x_i values.

Figure 4 shows a comparison of the model results (relative tangential component of velocity) with the analytical formulations proposed in [7] and [9].

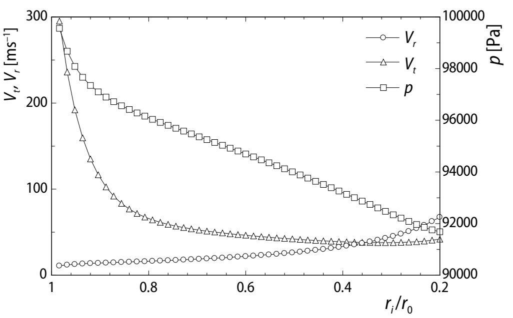

Figure 3. Pressure, tangential and radial velocity components *vs.* non-dimensional radius

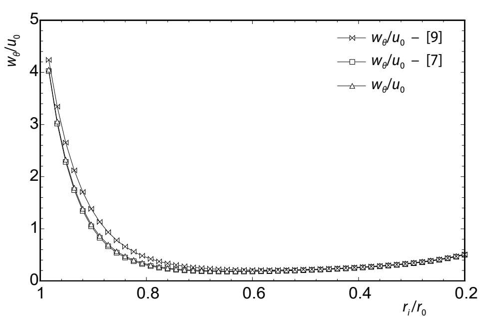

Figure 4. Comparison between model and literature; tangential component of relative velocity

Performance of the Tesla turbine rotor

Performance indicators

In order to assess the performance potential of the turbine, a parametric study needs to be performed. The parametric analysis should show the performance as a function of the main design variables, which are non-dimensionalized following common practice in turbomachinery [19]. All the results obtained in the parametric analysis refer to air as the working fluid.

Moreover, critical design parameters for the Tesla turbine were identified in the geometrical ratios (D_1/D_0) and (b_0/D_0): for output conditions critical performance indicators were identified as the exit kinetic energy and the absolute flow angle, which should be as low as possible, see tab. 2.

Overall performance results

The trend of the rotor efficiency, η, as a function of (D_1/D_0) and (b_0/D_0) is shown in fig. 5.

The rotor efficiency, η, is only slightly affected by different values of the exit diameter. With decreasing D_1/D_0, the larger kinetic energy at discharge, due to the higher axial component of velocity, appears to be somewhat compensated by the larger rotor surface available for momentum exchange between the fluid and the disks.

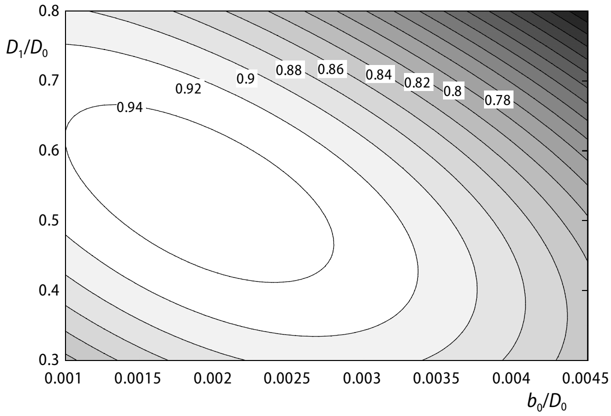

Figure 5. Rotor efficiency, η, *vs.* D_1/D_0 and b_0/D_0

On the other hand, the (b_0/D_0) parameter – the non-dimensional gap between two disks – strongly affects the efficiency of the rotor. This is due to the influence of the Reynolds number in the laminar flow regime, which can be best explained re-arranging its definition and remembering that $b = D_\mathrm{h}/2$:

$$\mathrm{Re} = \frac{\rho V_r D_\mathrm{h}}{\mu} = \frac{\dot{m}_c}{2\pi r b \rho}\frac{\rho D_\mathrm{h}}{\mu} = \frac{\dot{m}_c}{\pi r \mu} \tag{24}$$

Similarly, the trend of the load coefficient Ψ *vs.* (D_1/D_0) and (b_0/D_0) is shown in fig. 6. The Ψ is very sensitive to the reduction of (b_0/D_0), however, differently from rotor efficiency η it also shows a sensitivity to (D_1/D_0). The momentum exchange is favoured as the wet area is increased, nevertheless, the exit diameter should not exceed a certain limit, the penalty being an increase of the residual tangential velocity, leading to higher discharge losses. From the points of view of rotor efficiency, η, and load coefficient, Ψ, values of $0.35 < (D_1/D_0) < 0.45$ and $0.005 < (b_0/D_0) < 0.015$ appear recommendable.

An important parameter, strongly influenced by the gap between disks, is the absolute exit angle, fig. 7. In order to reduce it and render possible an efficient recovery of discharge kinetic energy, the exit fluid angle should be close to axial, $\alpha_1 \cong 0$. A reduction of the gap between the plates is definitely beneficial to this end. The decrease of α for smaller values of b_0 is due to the reduction of the tangential component, as well as to the increase in the radial component of absolute velocity. The reduction of tangential velocity, as can be noted from eq. (23), is due to the

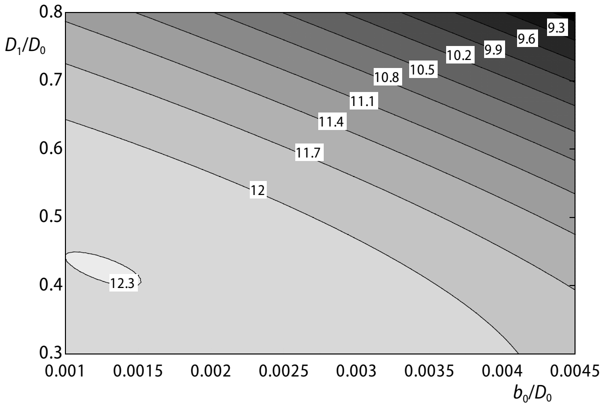

Figure 6. Rotor load coefficient, *Ψ*, *vs.* D_1/D_0 and b_0/D_0

increase of viscous momentum transfer for small values of b_0. On the other hand, the radial velocity increases because of the continuity, eq. (5).

The trend of the absolute velocity and of its components with variable gap is displayed in fig. 8. The absolute exit velocity has a minimum, determined by opposite trends with b_0/D_0 of the two components of velocity (radial and tangential). The minimum of the exit kinetic energy E_{kin1} corresponds to maximization of the rotor efficiency.

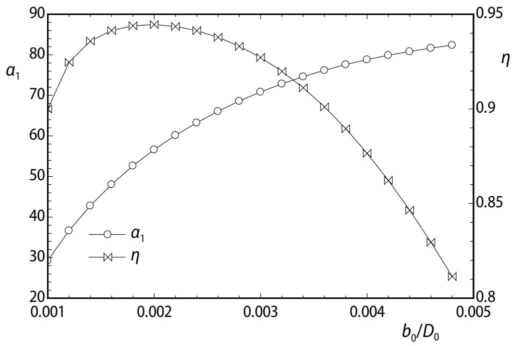

Figure 7. Exit fluid angle, *α*, and efficiency of the turbine *vs.* b_0/D_0, for D_1/D_0 = 0.44

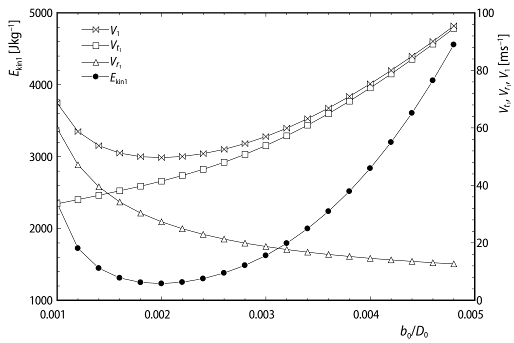

Figure 8. Exit kinetic energy *vs.* non-dimensional gap

As for the influence of the flow coefficient, the absolute exit angle and the efficiency are plotted against *Φ* in fig. 9. Increasing the flow coefficient, the absolute exit angle decreases. This is due to an increase of the radial component of the fluid, which therefore turns the fluid in the axial direction. If values of exit flow angles below 50° are sought, then a flow coefficient in the range *Φ* = 0.2 should be selected, under these conditions, the rotor efficiency is still high – in the range of 0.94.

The final geometry is summarized in tab. 2.

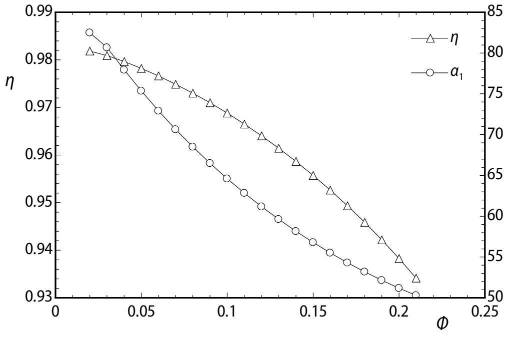

Figure 9. The α_1 and *η* *vs.* *Φ*

Table 2. Final geometry of Tesla rotor (working fluid = air)

Mass-flow rate	0.00194 kg/s
Rotational speed	6300 rpm
Inlet Mach number	1
Inlet diameter, D_0	0.1778 m
Exit diameter, D_1	0.0772 m
Gap, b_0	0.00032 m
Absolut exit angle, α_1	52°
Power produced for each channel	40.8 W
Exit Mach number	0.1168

Conclusions

An upgraded description of the Tesla turbine rotor flow was presented and validated against similar literature models. The new model includes variable density and applies a real fluid model (no incompressible fluid or perfect gas assumptions). Existing experience with prototypes of Tesla turbines has always dealt with air or steam as working fluid, so that the capability of modelling general fluids looks potentially attractive.

The model was applied to evaluate the sensitivity of performance to the most relevant design variables, that is: D_1/D_0, b_0/D_0, and the flow coefficient. The main calculated performance parameters analysed are the total-to-static efficiency and the work coefficient.

The results indicate that the Tesla rotor appears potentially competitive with other types of expanders, with special reference to efficiency.

Nomenclature

A – surface, [m^2]
b – gap between two discs, [m]
D – diameter, [m]
D_h – hydraulic diameter, [m]
E – kinetic energy, [Jkg^{-1}]
F – force, [N]
f – body force per unit mass, [ms^{-2}]
h – enthalpy, [Jkg^{-1}]
$\dot{m}_c$ – mass-flow rate, [kgs^{-1}]
p – pressure, [Pa]
Q – volume, [m^3]
Re – Reynolds number (relative flow)
r – local radius, [m]
rpm – rotational speed, [rpm]
T – temperature, [°C]
U – tangential velocity, [ms^{-1}]
V – absolute velocity, [ms^{-1}]
V_r – relative velocity, [ms^{-1}]
V_θ – tangential velocity, [ms^{-1}]
x – non-dimensional radius
w – relative velocity, [ms^{-1}]
W – power, [W]

Greek symbols

α – absolute flow angle, $[= \tan^{-1}(v_{\theta 1}/v_{r1})]$, [°]
β – relative flow angle, [°]
ζ – friction factor
η – total-to-static efficiency (rotor only), $\{= (V_{\theta 0}U_0 - V_{\theta 1}U_1)/[(h_0 - h_1) + V_0^2/2]\}$
μ – dynamic viscosity, [kgm^{-1}s^{-1}]
ν – kinematic viscosity, [m^{2}s^{-1}]
ρ – density, [kgm^{-3}]
τ – wall shear stress, [Pa]
Φ – flow coefficient, $(= v_{r0}/U_0)$
ψ – load coefficient, $[= (V_{\theta 0}U_0 - V_{\theta 1}U_1)/(U_0^2/2)]$
ω – rotational speed, [rads^{-1}]

Subscripts and superscripts

0 – rotor inlet value
1 – rotor outlet value
e – fluid element
i – point i
kin – kinetic
r – radial direction
t – time, [s]
w – wetted wall
z – axial direction
θ – tangential direction

References

[1] Tesla, N., Turbine, *U.S. Patent No. 1 061 206*, 1913
[2] Armstrong, J. H., An Investigation of the Performance of a Modified Tesla Turbine, M. S. thesis, Georgia Institute of Technology, Atlanta, Geo, USA, 1952
[3] Rice, W., An Analytical and Experimental Investigation of Multiple-Disk Turbines, *ASME Journal of Engineering for Power*, *87* (1965), 1, pp. 29-36
[4] Hoya, G. P., Guha, A., The Design of a Test Rig and Study of the Performance and Efficiency of a Tesla Disc Turbine, *Proceedings, Institution of Mechanical Engineers, Part A: Journal of Power and Energy*, *223* (2009), 4, pp. 451-465
[5] Guha, A., Smiley, B., Experiment and Analysis for an Improved Design of the Inlet and Nozzle in Tesla Disc Turbines, *Proceedings, Institution of Mechanical Engineers, Part A: Journal of Power and Energy*, *224* (2009), 2, pp. 261-277
[6] Neckel, A. L., Godinho, M., Influence of Geometry on the Efficiency of Convergent-Divergent Nozzles Applied to Tesla Turbines, *Experimental Thermal and Fluid Science*, *62* (2015), Apr. pp. 131-140

[7] Carey, V. P., Assessment of Tesla Turbine Performance for Small Scale Rankine Combined Heat and Power Systems, *Journal of Eng. for Gas Turbines and Power*, *132* (2010), 2, 122301
[8] Carey, V. P., Computational/Theoretical Modeling of Flow Physics and Transport in Disk Rotor Drag Turbine Expanders for Green Energy Conversion Technologies, *Proceedings,* ASME 2010 International Mechanical Engineering Congress and Exposition, Fairfield, Conn., USA, 2011, Vol. 1, pp. 31-38
[9] Guha, A., Sengupta, S., The Fluid Dynamics of the Rotating Flow in a Tesla Disc Turbine, *European Journal of Mechanics B/Fluids*, *37* (2013), Jan.-Feb., pp. 112-123
[10] Sengupta, S., Guha, A., A Theory of Tesla Disc Turbines, *Proceedings, Institution of Mechanical Engineers, Part A; Journal of Power and Energy*, *226* (2012), 5, pp. 650-663
[11] Lemma, E., *et al*., Characterisation of a Small Viscous Flow Turbine, *Experimental Thermal and Fluid Science*, *33* (2008), 1, pp. 96-105
[12] Sengupta, S., Guha, A., Analytical and Computational Solutions for Three-Dimensional Flow-Field and Relative Pathlines for the Rotating Flow in a Tesla Disc Turbine, *Computers & Fluids*, *88* (2013), Dec., pp. 344-353
[13] Romanin, V. D., *et al*., Experimental and Analytical Study of Sub-Watt Scale Tesla Turbine Performance, *Proceedings,* ASME 2012 International Mechanical Engineering Congress & Exposition, Houston, Tex., USA, 2012, Vol. 6, pp. 1005-1014
[14] Krishnan, V. G., *et al*., Design and Scaling of Microscale Tesla Turbines, *Journal of Micromechanics and Microengineering*, *23* (2013), 12, pp. 1-12
[15] Guha, A., Sengupta, S., Similitude and Scaling Laws for the Rotating Flow between Concentric Discs, *Proceedings, Institution of Mechanical Engineers, Part A; Journal of Power and Energy*, *228* (2014), 4, pp. 429-439
[16] Guha, A., Sengupta, S., The Fluid Dynamics of Work Transfer in the Non-Uniform Viscous Rotating Flow Within a Tesla Disc Turbomachine, *Physics of Fluids*, *26* (2014), 3, 033601
[17] Sengupta, S., Guha, A., Flow of a Nanofluid in the Microspacing Within Co-Rotating Discs of a Tesla Turbine, *Applied Mathematical Modelling*, *40* (2016), 1, pp. 485-499
[18] Klein, S. A., Nellis, G. F., *Mastering EES*, F-Chart Software, Madison, Wis., USA, 2012
[19] Dixon, S., L., *Fluid Mechanics and Thermodynamics of Turbomachinery,* 5th ed., Pergamon Press, Oxford, UK, 2005

Paper submitted: June 1, 2016
Paper revised: March 9, 2018
Paper accepted: May 13, 2018